JOURNAL OF MAGNETIC RESONANCE **90**, 71–89 (1990)

Flow-Velocity Imaging from Linear Regression of Phase Images with Techniques for Reducing Eddy-Current Effects

A. CAPRIHAN, S. A. ALTOBELLI, AND E. BENITEZ-READ

Lovelace Medical Foundation, 2425 Ridgecrest Drive, SE, Albuquerque, New Mexico 87108

Received January 25, 1989; revised March 16, 1990

Proton NMR velocity images are obtained, in which the intensity is proportional to a component of flow velocity, by velocity encoding the phase images. These velocity images of flowing water are constructed by a voxel-by-voxel linear regression of image phase versus m_1, a parameter which is proportional to the first moment of the magnetic field gradient and which is used to encode the constant but spatially varying velocity. At each image voxel the standard deviation of the velocity estimate is calculated and plotted as an image. This standard-deviation image provides a check on the accuracy of velocity calculations. The errors in the velocity calculations caused by eddy-current-induced phase shifts are discussed and two methods for reducing these errors are proposed. A pulse sequence with lower eddy-current sensitivity can be chosen and, in addition, static spins can be used for phase referencing. A pulse sequence consisting of time-shifted π pulses is shown to have lower eddy-current sensitivity than other pulse sequences considered. Phase referencing can be used with all methods of velocity encoding and reduces the eddy-current-induced velocity errors.

A number of NMR methods for fluid-velocity measurement which depend on the proportionality between spin phase and velocity for a given gradient first moment have been proposed. Among others, they consist of a standard imaging sequence in which velocity encoding is done automatically in the read-out direction (*1*), a method which depends on the use of bipolar gradients (*2*), a method which encodes velocity by shifting the gradient pulses (*3*) rather than by changing the amplitude of the gradient pulses, and another which codes flow during a selective π RF pulse (*4*). In these methods, the general principle of which has been discussed in the imaging context by Moran (*5*), the phase shift of the spins moving with a constant velocity between the $\pi/2$ pulse and the time of spin-echo measurement is a linear function of the first moment of the gradient (m_1) and of the velocity component along the gradient (*2*). This results in the phase of an image voxel also having a linear dependence on the first moment of the gradient and the velocity component along the gradient from which the velocity information can be calculated.

In this paper, we discuss some of the problems in calculating the velocity from the phase of an image voxel as well as a new procedure for calculating the velocities by linear regression. In the Fourier transform methods of NMR imaging, magnetic field gradients must be switched on and off and eddy-current effects are always present. A major problem in velocity imaging is the phase error caused by these eddy currents which depend on the first moment of the gradient. Although there are ways to reduce

0022-2364/90 $3.00

these effects by hardware modifications to the gradient coil itself, for example, by self-shielded gradient coils (*6*) or smaller gradient coils, and by shaping of the voltage applied to gradient coils (*7*), eddy-current effects remain a major problem. We will discuss methods of reducing errors in velocity calculations due to eddy currents which are independent of hardware modifications.

Our method of velocity imaging consists of performing NMR imaging experiments for different values of the first moment of the gradient and calculating the velocity by a voxel-by-voxel linear regression of the signal phase. At each voxel, we can also calculate the standard deviation of our velocity estimate and get an idea of the velocity measurement accuracy. In addition, methods of statistical hypothesis testing can be used to decide whether spins in any voxel are static or moving.

We use two independent approaches to reduce the severity of the eddy-current-induced phase errors which depend on m_1 and cause the static spins to have an apparent nonzero velocity. We first show an alternative method, similar to that of Naylor *et al.* (*3*), of varying the first moment of the gradient by time shifting the π RF pulses with reduced eddy-current sensitivity, which results in more accurate velocities than other velocity-encoding schemes. We next suggest a method of phase referencing to reduce the contribution of the eddy-current-induced phase shifts which depend on m_1. This consists of referencing the phase image of flowing spins to a phase image of stationary spins. A number of variations will be compared for this purpose. The phase referencing and the velocity encoding are independent so they can both be used simultaneously to reduce eddy-current effects.

METHODS FOR VELOCITY IMAGING

A NMR spin-echo imaging experiment begins with an RF pulse (selective or non-selective) which tips the magnetization into the transverse plane. If these observable spins move in the presence of magnetic field gradients, the phase and the amplitude of the spin echo are altered compared to those of static spins. These effects depend on the component of the velocity and other higher-order derivatives of position in the direction of the gradient. If we assume that the velocity is constant during the measurement process, i.e., between the $\pi/2$ RF pulse and the time of spin echo, and the effective velocity-encoding gradient has zero area ($\int G(t)dt = 0$), the NMR signal from a voxel at position r, after 2D Fourier transformation of sampled echoes, is given by

$$S_r(m_1) = \int e^{-i\gamma m_1 v} p_r(v) dv, \qquad [1]$$

where γ is the gyromagnetic ratio, $m_1 = \int tG(t)dt$ is proportional to the first moment of the gradient, and $p_r(v)$ is the velocity-density function (the number of spins with velocities between v and $v + dv$) within the voxel. In this article, we refer to m_1 as the first moment of the gradient even though m_1 is unnormalized so it is only proportional to the first moment.

The integral in Eq. [1] is independent of spin position because the time integral of the velocity-encoding gradient is zero. $S_r(m_1)$ is thus the Fourier transform of the velocity-density function $p_r(v)$. If the experiment is done for several values of m_1, an

inverse Fourier transform of $S_r(m_1)$ will yield $p_r(v)$. The step size of m_1 and the number of steps required to define $p_r(v)$ depend on the velocity range in the voxel and the desired resolution of the velocity-density function.

Instead of the Fourier transform approach, we adopt a parametric, or model, approach to velocity estimation. We assume that $p_r(v)$ can be described by a model with parameter values varying from voxel to voxel and our goal is to estimate these parameters. If the model is described by a small number of parameters, then the number of experiments required to estimate these parameters is also small.

If the velocity-density function $p_r(v)$ is symmetric around the mean velocity $V(r)$, then

$$S_r(m_1) = e^{-i\gamma m_1 V(r)} \int \cos(\gamma m_1 v) p_r(v + V(r)) dv. \qquad [2]$$

Since the integral is a real function for a symmetric velocity-density function, the phase of the signal at that voxel depends only on the mean velocity within the voxel. If we assume $p_r(v)$ is uniformly distributed between $V(r) - \Delta(r)$ and $V(r) + \Delta(r)$, then

$$S_r(m_1) = e^{-i\gamma m_1 V(r)} \{\sin(\gamma m_1 \Delta(r))\} / \gamma m_1 \Delta(r). \qquad [3]$$

Thus for uniform velocity-density function, the amplitude of the NMR signal depends on the spread of the velocity within the voxel. This reduction in signal amplitude with increased variance of velocity-density function is a general result and can also be shown for other velocity-density functions.

We now discuss a method of measuring velocity profiles based on the phase of the NMR image. If the velocity-density function in a voxel is symmetric, then the phase of the image at the voxel r is linearly proportional to the first moment of the gradient and the mean velocity within the voxel, i.e.,

$$\phi(r) = \gamma m_1 V(r). \qquad [4]$$

This is a well-known result and was used by Dumoulin and Hart (*2*), who subtracted phase images taken with two equal and opposite values of m_1 to obtain an angiogram. We perform NMR imaging experiments for different values of m_1, and $V(r)$ is obtained by linear regression of phase versus m_1. A velocity image can be constructed in which each voxel has intensity proportional to velocity calculated in this way.

If the velocity distribution is not symmetric within a voxel then the velocity $\hat{V}$ as measured by the phase method will not equal the average spin velocity $V(r)$. The accuracy of the assumption that the velocity-density function is symmetric depends on the size of the voxel and the type of flow. If the voxel is a point then it can have only one velocity and the assumption is valid with $\Delta(r) = 0$. If the flow is laminar and the voxel size is large enough to include the cross section of the vessel, then the density function is also uniform and symmetric.

In order to avoid aliasing problems, the step change for m_1 should be chosen so that the corresponding step change in phase $\phi(r)$ is less than π radians for a given maximum expected velocity. In addition, phase unwrapping will not be required if we also ensure that the absolute value of phase is less than π radians for the maximum

expected velocity and for all values of m_1 used. Phase unwrapping, if necessary, can be done with appropriate computer algorithms.

EDDY-CURRENT ANALYSIS

We will now show that velocity estimation errors caused by eddy currents depend on the method used for velocity encoding. In practice the eddy currents induced by switching gradients are multiexponential in time with components from closer metal surfaces having faster decay times and those from the cold magnet parts decaying slowly. The eddy currents also have spatial variations which depend on the magnet geometry. In particular, not only are the eddy currents different for G_z compared to the transverse gradients G_x and G_y, the eddy-current effects from each gradient coil, e.g., G_x, depend on space and can also have components along other axes, i.e., y and z. These eddy currents, in effect, cause a time- and space-dependent error in the homogeneous field B_0 and in the applied gradient.

Although these additional fields due to eddy currents have temporal dependences that are multiexponential at any point in space, we consider only a simple, one-exponential-time behavior. We will evaluate the eddy-current sensitivity $S(P)$ to changes in a gradient parameter P of a velocity-encoding method by calculating the ratio of the change in phase caused by eddy currents to the change in the phase caused by the velocity. We define

$$S(P) = \frac{\partial \phi_e / \partial P}{\partial \phi_v / \partial P}, \qquad [5]$$

where $\phi_e(P)$ is the accumulated phase at echo time due to the eddy current with gradient parameter P and $\phi_v(P) = \gamma V m_1(P)$ is the phase caused by the spins flowing at velocity V in a velocity-encoding gradient with first moment $m_1(P)$. The parameter P can be the gradient amplitude, time, or duration. In general, $S(P)$ will be a nonlinear function of P although it is linear for amplitude modulation of the gradients. For simplicity, we will compare $S(P = 0)$ for a number of different velocity-encoding methods but $S(P)$ must be considered for all P for a complete study.

From Eq. [5], $S(P)$ is inversely proportional to V, which means that the relative error in velocity estimation due to eddy currents will be smaller for larger velocities. From now on we will calculate $S(P)$ for $V = 1$ cm/s, which implies that

$$S(P) = \frac{\partial \phi_e / \partial P}{\gamma \partial m_1 / \partial P} = \frac{\partial \phi_e / \partial m_1}{\gamma}. \qquad [6]$$

$S(P)$ also represents the apparent nonzero velocity, in centimeters per second, of stationary spins caused by eddy-current-induced phase errors. If flowing spins are present then this velocity error will be added to the correct velocity. Another significance of Eq. [6] is that the velocity estimation is in error only if the eddy-current-induced phase shifts are a function of m_1.

We will calculate $S(P)$ for the velocity-encoding schemes shown in Fig. 1, even though these are not velocity-compensated gradient sequences as used in our experiments, because they will illustrate the differences between the three methods of velocity encoding. For the sequence in Fig. 1a the first moment of the gradient is changed by

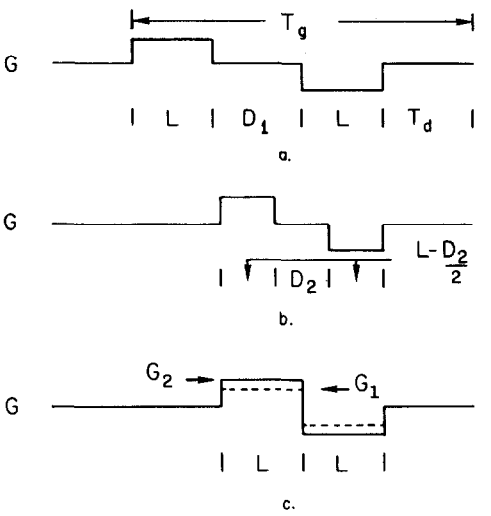

FIG. 1. Three different methods of changing the first moment of the velocity-encoding gradient to be compared for their eddy-current sensitivity: (a) by shifting the first pulse, (b) by changing the duration of both pulses, or (c) by changing the gradient amplitudes.

shifting the position of the first gradient pulse with respect to the second, in Fig. 1b by changing the widths of the two pulses, and in Fig. 1c by changing their amplitudes. The effect of eddy currents on signal phase is compared at a fixed time after the end of the last gradient pulse.

Consider the scheme of Fig. 1a. If $B_e(t)$ is the magnetic field at any spatial position r caused by eddy currents, the phase at echo time due to this error is given by

$$\phi_e(D_1) = \gamma \int_0^{T_g} B_e(t)dt, \qquad [7]$$

where T_g is the time from the start of the velocity-encoding gradient to the center of the echo. We assume that the gradient pulses are step functions, that the eddy currents generated by each gradient step are proportional and opposite in sign to the step size, and that they are single exponential functions with time constant $1/\beta$. Then for two bipolar gradient pulses of duration L separated by the independent variable D_1 as shown in Fig. 1a,

$$B_e(t) = kG(-e(t) + e(t - L) + e(t - L - D_1) - e(t - 2L - D_1)), \qquad [8]$$

where G is the gradient amplitude, k is a proportionality constant, and $e(t) = e^{-\beta t}u(t)$ with $u(t) = 1$ for $t \geq 0$ and zero otherwise. After integration

$$\phi_e(D_1) = (\gamma kG/\beta)e^{-\beta T_d}(1 - e^{-\beta L})(1 - e^{-\beta(L+D_1)}), \qquad [9]$$

where T_d (Fig. 1a) is the time measured from the end of the last gradient pulse to the center of the echo. For this case, $m_1(D_1) = GL(L + D_1)$ and

$$S(D_1 = 0) = (k/L)e^{-\beta T_d}e^{-\beta L}(1 - e^{-\beta L}), \qquad [10]$$

where $S(D_1 = 0)$ is a shorthand notation for $S(D_1)$ at $D_1 = 0$.

If the observation time were at infinity, i.e., $T_d \rightarrow \infty$, then the error due to the eddy currents is zero and this is also true for other methods of velocity encoding. For simplicity, we will now assume $T_d = 0$; in other words, we will calculate the eddy-current errors at the end of the last velocity-encoding gradient pulse. In this case, Eq. [10] becomes

$$S(D_1 = 0) = (k/L)e^{-\beta L}(1 - e^{-\beta L}). \quad [11]$$

A similar calculation for Fig. 1b, where the total length of the velocity-encoding gradient is kept fixed at $2L$ and the width of the bipolar pulses is changed as a function of D_2, gives

$$\phi_e(D_2) = (\gamma kG/\beta)(1 - e^{-\beta(L-D_2/2)})(1 - e^{-\beta(L+D_2/2)}) \quad [12]$$

and $m_1(D_2) = G(L - D_2/2)(L + D_2/2)$. Then

$$S(D_2 = 0) = (k/L)\beta L e^{-\beta L}. \quad [13]$$

For the bipolar gradient pulse pair whose amplitude is changed to obtain different m_1, as shown in Fig. 1c, we get

$$\phi_e(G) = (\gamma kG/\beta)(1 - e^{-\beta L})^2 \quad [14]$$

and $m_1(G) = GL^2$, which lead to

$$S(G = 0) = (k/L)\frac{(1 - e^{-\beta L})^2}{\beta L}. \quad [15]$$

Since both $\phi_e(G)$ (Eq. [14]) and $m_1(G)$ are linear functions of G, $S(G)$ is actually independent of G.

These three methods (Figs. 1a, 1b, and 1c) of velocity encoding can be implemented equally well with π pulses as shown in Fig. 2a. The analysis of eddy-current errors with π pulses is slightly different because the phase shift accrued due to eddy currents will now be inverted by the π pulse. For this example, the sequence is flow compensated, i.e., $m_1 = 0$, when $D_3 = 0$, and we have

$$\phi_e(D_3) = (\gamma kG/\beta)(h_{a1}(B) + h_{a2}(B, D_3)), \quad [16]$$

where $h_{a1}(B)$ is a function independent of D_3 and

$$h_{a2}(B, D_3) = e^{-\beta L}(2e^{\beta D_3}e^{-\beta B/2}(1 - e^{-\beta(2L+B)}) + e^{-\beta D_3}(1 - e^{-\beta B})(1 + e^{-\beta(2L+B)})). \quad [17]$$

Similarly, for the equivalent sequence with gradient reversals instead of π pulses (Fig. 2b), we get

$$\phi_e(D_3) = (\gamma kG/\beta)(h_{b1}(B) + e^{-\beta L}e^{-\beta D_3}(1 + e^{-\beta B})(1 - e^{-\beta(2L+B)})), \quad [18]$$

where $h_{b1}(B)$ is independent of D_3. For both these cases, $m_1(D_3) = 2GD_3(2L + B)$ and the eddy-current sensitivity for the sequence with π pulses (Fig. 2a) is given by

$$S(D_3 = 0) = (k/L)e^{-\beta L}(2e^{-\beta B/2}(1 - e^{-\beta(2L+B)}) - (1 - e^{-\beta B})(1 + e^{-\beta(2L+B)})), \quad [19]$$

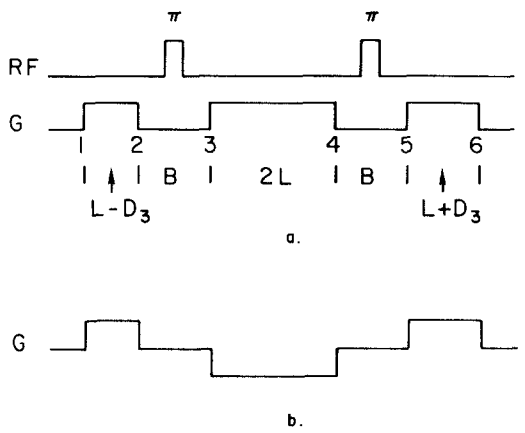

FIG. 2. Comparison of flow-compensated velocity-encoding methods. If $D_3 = 0$, the sequence is flow-compensated because the first moment of the gradient is zero. Part a is the method of velocity encoding used in our experiments and b is an equivalent gradient-refocusing method without π pulses. The slice selection in y reduces static spin signals outside the tube, when present. It is flow compensated for a flow in the y direction.

whereas it is

$$S(D_3 = 0) = -(k/L)e^{-\beta L}(1 + e^{-\beta B})(1 - e^{-\beta(2L+B)}) \qquad [20]$$

for the gradient reversal sequence, Fig. 2b.

Equations [19] and [20] show that the eddy-current sensitivity for Figs. 2a and 2b is identical for $B = 0$ but is smaller for velocity encoding with a π pulse (Fig. 2a) when $B \neq 0$. In fact the two terms in Eq. [19] have opposite signs so that for some appropriate choice of B, which depends on D_3, the sensitivity can be zero. In Fig. 2a, the eddy-current-induced phase error (Eq. [17]) has one component which depends on $e^{\beta D_3}$ (caused by transition 1 in Fig. 2a) and another component which depends on $e^{-\beta D_3}$ (caused by transitions 2 to 5 in Fig. 2a). As D_3 is increased, the π pulse comes closer to transition 1 causing its eddy-current contribution to increase as $e^{\beta D_3}$. The eddy-current contributions of transitions 2 to 5 do not depend on the shift of the π pulses, but the time to the point of eddy-current-error calculation (transition 6) increases with D_3, causing the eddy-current contribution to decrease as $e^{-\beta D_3}$. Thus for a given change in D_3, the changes in the two contributions to ϕ_e are of opposite signs, permitting a choice of B to give zero error.

If βL is sufficiently large, the term $e^{-\beta(2L+B)}$ can be neglected, and the sensitivity in Eq. [19] is zero for $\beta B = -2 \ln(\sqrt{2} - 1) \approx 1.76$. This result, however, is based on a number of assumptions. The optimum value of B depends on β, the time constant defining the eddy-current behavior. In general, the eddy currents are multiexponential and with spatial dependences, and the time constants and their spatial variations are generally not known. The pulse sequence with the π pulses, Fig. 2a, promises to have improved eddy-current sensitivity as demonstrated by a first-order model for eddy currents but the sequence parameters would have to be optimized experimentally in each situation.

We compare the relative eddy-current sensitivities of the four velocity-encoding methods (Figs. 1a, 1b, 2a, and 2b) to that of the amplitude-modulation method of Fig. 1c. The comparison is independent of k/L and the results with $T_d = 0$ are shown in Table 1. A smaller sensitivity ratio means that velocity calculations have smaller errors due to eddy-current-induced phase shifts. The top two lines of the table show that the time-shifting and changing-pulse-width velocity-encoding methods perform better than the amplitude-modulation method. The bottom four lines of the table show that, with proper choice of parameter B, the π-pulse method (Fig. 2a) has lower sensitivity to eddy currents than the method without π pulses (Fig. 2b) and, in fact, it has the least sensitivity to eddy currents among the methods compared.

There are a number of other considerations and methods of velocity encoding which were not discussed. The method of analysis presented should be applicable to these other cases. In all our previous comparisons T_d was put equal to 0; this was possible because the eddy-current sensitivity $S(P)$ decreased as $e^{-\beta T_d}$ for all the velocity-encoding methods. This implies that the velocity encoding should be done as early as possible as compared to the time of echo measurement. Another related conclusion is that, if the gradient strengths present no problems, then for a fixed velocity-encoding time it is better to use short, intense, gradient pulses, as early as possible. The sensitivity improves because the eddy-current effects decrease exponentially during the time saved by shorter velocity-encoding pulses, more than compensating for the increase in eddy-current effects caused by shorter gradient pulses.

DATA ANALYSIS

There are two independent components to this section. Because our velocity measurements are based on the phase increments imparted to the nuclei by the motion,

TABLE 1

Sensitivity of Velocity-Encoding Schemes to Eddy-Current Effects Relative to the Standard Velocity-Encoding Scheme of Varying the Bipolar Velocity-Encoding Gradient Pulse Amplitudes

Sequence	Figure	Sensitivity ratio	
		$\beta L = 3$	$\beta L = 5$
Time shift	1a	0.156	0.034
Width change	1b	0.495	0.171
Flow-compensated π-pulse refocusing, $\beta B = 0$	2a	0.083	0.019
Flow-compensated π-pulse refocusing, $\beta B = 1.76$	2a	2.87 E-05	1.16 E-05
Flow-compensated gradient refocusing, $\beta B = 0$	2b	−0.083	−0.019
Flow-compensated gradient refocusing, $\beta B = 1.76$	2b	−0.037	−0.009

Note. The numbers in the table are $S(D_n = 0)/S(G = 0)$, where the D_n's are the various delays defined in Figs. 1a, 1b, 2a, and 2b (see text). The comparison is shown for $\beta L = 3$ and $\beta L = 5$, which correspond to eddy currents being less than 5 and 1%, respectively, of their initial value.

we need to know the phase shifts caused by the eddy currents (and all other causes, if any) in the absence of flow. The phase-referencing schemes we describe below are designed to obtain and eliminate such eddy-current-induced errors in the phase images. The discussion of phase referencing will be followed by the method of linear regression for velocity estimation.

After baseline correction and 2D FFT (fast Fourier transformation), an important step in the calculation of complex images consists of phasing the image to make the imaginary part of the image as small as possible. In our spectrometer/imager, this phase correction consists of modifying each complex pixel value C_{mn} to $C_{mn}e^{i\phi_c}$, where $\phi_c = P_a + 2P_b m/N + 2P_{by} n/N$ with P_b the linear phase correction in the read-out direction and P_{by} the linear correction in the phase-encoding direction. The need to correct the phase exists regardless of eddy currents, but eddy-current effects affect the phase corrections. If the velocity-encoding gradient is in the read-out gradient direction, then the primary effect of eddy currents is seen as a shift in the echo which changes the value of P_b needed for phasing the image. If the velocity-encoding gradient is in the phase-encoding direction, then the primary effect of eddy currents is to shift the echo in the phase-encoding direction which changes the value of P_{by} needed for phase correction. Finally, if the velocity-encoding direction is along the slice-selection direction then the primary effect of eddy currents is to reduce the signal intensity. We use static images to find the values for the constants P_a, P_b, and P_{by} at each velocity-encoding step. If eddy-current effects were absent, these constants would be the same for all velocity-encoding steps.

Because the calculation of phase requires a division, we calculate it only in regions where the object is defined, i.e., in regions of nonzero signal-to-noise ratio. In order to accomplish this, we use the magnitude of the velocity-compensated image, i.e., the one with $m_1 = 0$ and which has the least signal loss due to phase incoherence, as a mask to define object boundaries. This image, which we call the flow-compensated magnitude image, does not depend on the phase correction ϕ_c. The appropriate region is that having signal intensity above some threshold. For the experiments discussed in this paper the threshold was chosen to be 0.05 times the maximum image intensity. This method of defining regions for phase calculation allows phases to be calculated from within an object even if the signal is small for an image taken with a large gradient first moment m_1.

We will compare a number of different ways for phase referencing by projection images of two tubes, one with flowing water and the other with stationary water. Phase referencing consists of applying a correction to the phase image so that the eddy-current-induced phase shifts which depend on m_1 are canceled. The first method consists of finding an appropriate P_a and P_b, for each velocity-encoding step, from a one-dimensional static image made without phase encoding. The value P_{by} is held constant. This method requires that the flow in the object being studied be controlled, and additional one-dimensional experiments for each value of m_1 with no flow be taken. This approach will work if a change in m_1 does not change the eddy-current-induced phase shifts in the phase-encoding direction. The following method attempts to relax this assumption.

For the second method, we take images with no flow for each value of m_1 and calculate P_a, P_b, and P_{by}, which are then applied to the corresponding images with

flow. This method, as before, requires that the flow in the object can be controlled, so that static images can be taken. Here we are assuming that the change in phase error induced by the change in m_1 is linear in the two-dimensional image space. If this is not the case, then the following third method will be better.

The experiment is exactly the same as the second method, but now the phase of the image with no flow is subtracted from the phase of the image with flow, for each value of m_1, to get the desired phase-referenced image. This method cancels spatially nonlinear changes in the phase error which change with respect to m_1.

The three methods of phase referencing described above have the disadvantage of requiring that the flow in the object being studied be stopped to take a static image for referencing purposes. This is not possible for some applications, including blood flow measurement. A method which does not require additional experiments without flow for phase referencing uses phantoms with static spins placed around the object where flow is being measured. Appropriate values of P_a, P_b, and P_{by} are then calculated from the phase image of these static spin phantoms for each value of m_1 and are applied to the regions with flow. We assume that the hyperplane as defined by the constants calculated from the static regions can be extrapolated to the region with flow and it can be extended to fitting a more complex surface to the phase image. This is a software correction, so that phase corrections may be independently made for each experiment, if necessary, without having to accumulate separate data for phase corrections.

The experimentally measured phase at any point r of the phased image can be expressed as

$$\phi(r) = a(r) + \gamma m_1 V(r) + \theta(r), \qquad [21]$$

where $a(r)$ is due to eddy currents and $\theta(r)$ is a random error. If phase referencing works as described, then the contribution of eddy currents $a(r)$ will be independent of m_1.

The phase image $\phi(r)$ can be calculated from an experiment with one value of m_1 but two or more images with different values of the first moment can be obtained to cancel the effects of eddy currents that are independent of m_1, and with three or more images we can reduce the effects of random noise $\theta(r)$. With three or more phase images, a linear regression is performed at each voxel, a confidence interval for $V(r)$ calculated, and the hypothesis $V(r) = 0$ tested.

For the regression model

$$\phi_i = a + \gamma m_{1i} V + \theta_i, \qquad i = 1, \ldots, n, \qquad [22]$$

and the velocity estimate, at any position r, is given by

$$\hat{V} = \frac{\sum (m_{1i} - \bar{m}_1)(\phi_i - \bar{\phi})}{\gamma \sum (m_{1i} - \bar{m}_1)^2}, \qquad [23]$$

where

$$\bar{m}_1 = \sum m_{1i}/n, \qquad [24]$$

$$\bar{\phi} = \sum \phi_i/n, \qquad [25]$$

and n is the number of experiments performed with different m_1's. In this regression model, we have assumed that the noise θ_i is normally distributed with zero mean and with variance σ^2. The unbiased estimate of σ^2 is

$$\hat{\sigma}^2 = \frac{1}{n-2}[\sum(\phi_i - \bar{\phi})^2 - \gamma^2\hat{V}^2 \sum (m_{1i} - \bar{m}_1)^2], \quad [26]$$

where $\hat{V}$ is normally distributed with mean V and variance

$$\sigma^2(\hat{V}) = \frac{\hat{\sigma}^2}{\gamma^2 \sum (m_{1i} - \bar{m}_1)^2}. \quad [27]$$

$\hat{V}$ in Eq. [23] has a t distribution with $n-2$ degrees of freedom; i.e., the distribution is a function of $n-2$. If a random variable x has a t distribution with n degrees of freedom, then $t_{n,\alpha}$ is defined by the probability that $x \leqslant t_{n,\alpha}$ is equal to α. The $(1-\alpha)$ level confidence interval for V is

$$(\hat{V} - t_{n-2,1-\alpha/2}\sigma(\hat{V}),\ \hat{V} + t_{n-2,1-\alpha/2}\sigma(\hat{V})) \quad [28]$$

and the probability that the unknown value of V lies in the interval defined by Eq. [28] is $(1-\alpha)$.

It is now easy to test the hypothesis that the velocity is zero in order to identify regions of static spins. The null hypothesis, $V = 0$, is rejected if $|\hat{V}| \geqslant t_{n-2,1-\alpha/2}\sigma(\hat{V})$. Increasing the number of experiments (n) will make the image smoother, decrease the standard deviation of velocity estimate, and also reduce the confidence interval.

The method of linear regression for velocity calculation was based on two assumptions; that the noise on phase calculation had normal distribution and that the phase shift due to eddy currents did not depend on m_1. If the noise is not normally distributed, we can still do a least-squares fit and estimate V by Eq. [23], but it will not be possible to give confidence intervals and test the hypothesis for $V = 0$. In fact, the phase shift due to eddy currents does depend on m_1, and these effects were compensated by phase referencing as discussed previously. The presence of m_1-dependent errors in phase will cause the measured velocity to be in error, which will not be detected by the method of linear regression but which can be monitored by velocity imaging a static phantom.

RESULTS

Experiments were done with a Nalorac Quest 4300 imager/spectrometer in an Oxford 1.9 T superconducting magnet with a 30 cm bore and a high-pass birdcage coil. The experiments in this paper have velocity encoding in the read-out (z) direction and we call these images projection or xz images. The slice selection in the y direction (shown in Figs. 3 and 4) is used to reduce the unwanted signal from stationary spins outside the tube when experiments are done in their presence.

We first compare the eddy-current sensitivity of two xz-projection velocity-encoding methods, one with time-shifted π pulses and the other with amplitude modulation. The pulse sequence shown in Fig. 3 is similar to Fig. 2a and has gradients with different amplitudes (G_1, G_2, and G_3) and duration (L_1, L_2, and L_3) in its three sections. The sequence is flow compensated ($m_1 = 0$) by adjusting the parameters L_1, L_2, and L_3 in the presence of slow flow. The gradient first moment is varied by shifting both the

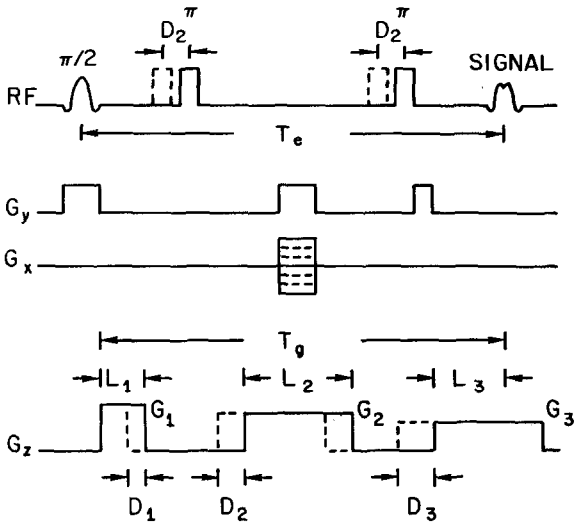

FIG. 3. A pulse sequence for xz-projection velocity imaging with flow in the z direction. The velocity encoding is done by time shifting the π pulses. The sequence can be flow compensated for some appropriate value of gradient amplitudes and their duration. If the shift D_2 is proportional to D_3, the first moment of the gradient is proportional to gradient amplitude (G_3) and its shift (D_3).

π pulses by D_2 and the gradients by D_1, D_2, and D_3 as shown in Fig. 3. For this case, the condition on gradients for the echo to form at T_e is

$$G_1L_1 + G_3L_3 = G_2L_2, \qquad [29]$$

and

$$G_1D_1 = G_3D_3. \qquad [30]$$

Then for a time shift specified by D_1, D_2, and D_3, the first moment is

$$m_1 = G_3D_3T_g - G_3D_3(L_1 + L_3) - G_3D_3(D_3 - D_1)/2 + G_2D_2L_2. \qquad [31]$$

If $G_1 = G_2 = G_3$, and $D_1 = D_2 = D_3$, then $m_1 = G_3D_3T_g$, which is the same as the first moment for the pulse sequence of Fig. 2a. The phase change for $G_3 = 0.1$ mT/cm, $D_3 = 100$ μs, $T_g = 20$ ms, and $V = 1$ cm/s is 3°. From Eq. [30], D_1 is proportional to D_3, so if D_2 is also chosen to be proportional to D_3, it follows from Eq. [31] that

$$m_1 = k_1G_1D_1 = k_2G_2D_2 = k_3G_3D_3, \qquad [32]$$

for some proportionality constants k_1, k_2, and k_3.

There is a similarity between this method for velocity encoding and that of Dixon (*8*) for chemical-shifting imaging. The major difference between the two methods is that we shift both the first and the second π pulse by the same amount while Dixon shifted only one π pulse. In our method, all the chemically shifted stationary spins rephase together at T_e without any phase shifts proportional to D_2 and the off-resonance frequency, because the change in phase caused by shifting the first π pulse by D_2 is exactly compensated by the change in phase caused by shifting the second π pulse.

Thus, for example, water and fat velocities will be correctly calculated without any chemical-shift artifacts.

The second sequence we consider is the amplitude-modulation velocity-encoding gradient as shown in Fig. 4. In this implementation the value of G_v can be adjusted to flow compensate the sequence. Then for a step change G_s in G_v

$$m_1 = G_s L T_g. \qquad [33]$$

In order to compare these two methods of velocity encoding, shown in Figs. 3 and 4, for eddy-current effects, one-dimensional projection images of a 9 cm long section of a 1.75 cm i.d. tube with stationary water are shown in Fig. 5. For both sequences, the echo time T_e was 30 ms, the read-out gradient was 0.05 mT/cm, and no y slice selection was used. Copper shields were used to define the section boundaries in the z direction. On the left side of Fig. 5 we have phase images from the amplitude-modulated pulse sequence of Fig. 4 and on the right side from the time-shifted pulse sequence of Fig. 3. Figures 5a and 5d are two images with $m_1 = 0$, and Figs. 5b and 5e are two images with m_1 corresponding to a phase shift of 28° for a velocity of 1 cm/s. The change in phase image between Figs. 5d and 5e is smaller than the change between Figs. 5a and 5b, demonstrating a lower eddy-current sensitivity of the time-shifted method. If the eddy-current-induced phase shifts did not depend on m_1, the two figures compared for each pulse sequence would be the same.

Next we apply a linear phase correction to Figs. 5b and 5e, obtaining Figs. 5c and 5f from Figs. 5b and 5e, respectively. It can be seen that the images corrected in this way are more like the $m_1 = 0$ images of Figs. 5a and 5d, showing that linear phase adjustment reduces the errors due to eddy currents. After phase adjustment, the eddy-current-induced errors for the two pulse sequences are similar, with the errors being larger at the ends of the object. A possible cause of this is that the eddy-current effects are not linear in our magnet. Thus with phase referencing, any reasonable velocity-

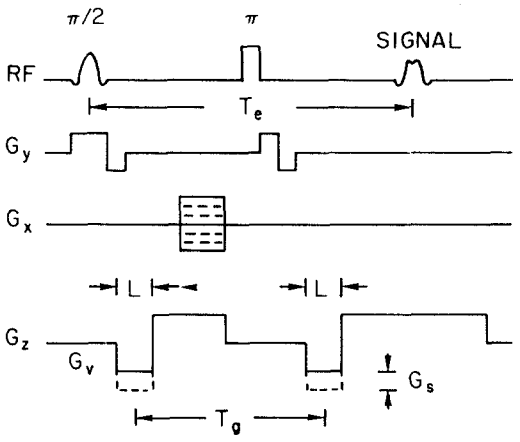

FIG. 4. A pulse sequence for xz-projection velocity imaging with flow in the z direction. The velocity encoding is done by amplitude modulation of an effective bipolar pulse. The sequence can be flow compensated for some appropriate value of G_v.

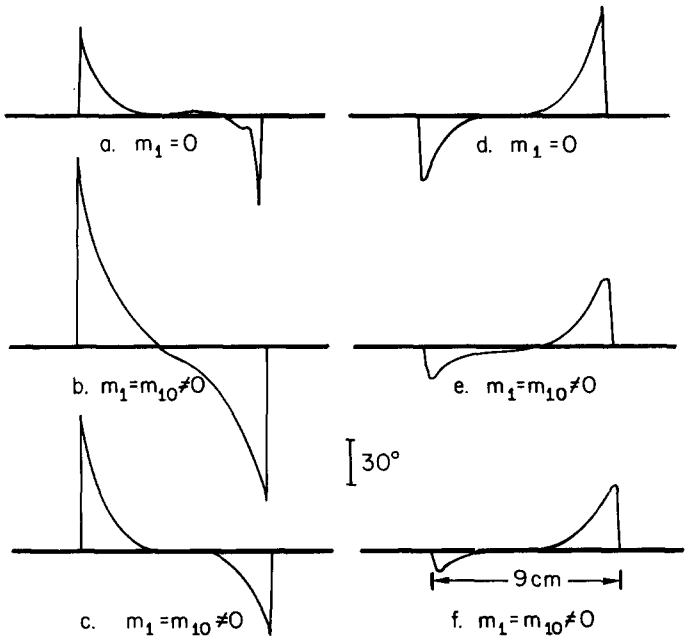

FIG. 5. The time-shifting and amplitude-modulation velocity-encoding schemes are compared for their sensitivity to eddy-current errors. These are one-dimensional phase images of a 9 cm long section of a 1.75 cm i.d. tube with static water. On the left are the phase images obtained from the amplitude-modulated pulse sequence of Fig. 4 and on the right from the time-shifted sequence of Fig. 3. Parts a and d are phase images with $m_1 = 0$ and b and e are those with a nonzero value of m_1. Parts c and f are obtained by applying linear phase corrections to b and e, respectively.

encoding method will perform equally well but, if phase referencing cannot be done, either because of inconvenience of placing stationary phantoms or due to the impossibility of doing additional images with zero flow, then a pulse sequence with lower sensitivity to eddy currents will perform better.

In Fig. 6 we show projection velocity images of water flowing at 8 cm/s (Reynold's number, Re = 1400) in a 1.75 cm i.d. cylindrical tube alongside a 1 cm i.d. tube filled with stationary water. A 9 cm long section of these tubes has been imaged. The time-shifted pulse sequence of Fig. 3 was used with the read-out gradient G_3 equal to 0.05 mT/cm and its first moment was varied by choosing five values of D_3 in steps of 200 μs around the position where the first moment of the gradient was equal to zero. The step D_2 was kept equal to D_3 and the step D_1 was adjusted experimentally to satisfy Eq. [30]. A phase shift of approximately 4° for a velocity of 1 cm/s was obtained with a shift of 200 μs. The echo time T_e was equal to 30 ms. Five phase images were collected with different values of m_1 centered around the flow-compensated image with $m_1 = 0$, as described earlier. The velocity was calculated by linear regression at each voxel. The flow-compensated magnitude image, which defines the region where the phase is calculated, is shown in Fig. 6a. The curvature of the outside edges of the tube is due to the nonlinearities in magnetic field gradients. In Fig. 6b, the intensity

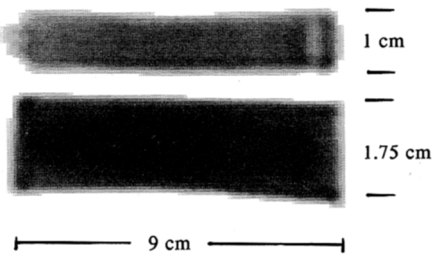

a. Flow compensated magnitude image.

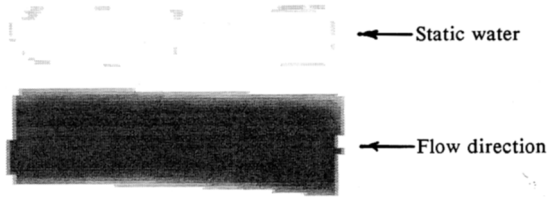

b. Velocity image.

FIG. 6. Projection velocity images, obtained in 9 cm long tubes of water by the time-shifted pulse sequence of Fig. 3. The larger 1.75 cm i.d. cylindrical tube has water flowing from right to left at 8 cm/s and the narrower cylindrical tube of 1 cm i.d. has stationary water. Five experiments were done with different values of m_1, and the velocity was calculated by linear regression at each voxel. Part a is the magnitude image for the flow-compensated gradient ($m_1 = 0$), whereas b is the velocity image obtained after linear regression. As expected, the image of the smaller tube shows zero velocity, except for some small errors at the upper edge of the tube.

is proportional to the velocity, so the tube with static water has almost zero intensity. The small error at the object boundaries is probably due to errors in phase caused by magnetic field susceptibility and small values of signal at the tube edge. The fact that phase referencing has eliminated the systematic errors due to eddy currents is verified from the zero-intensity velocity image of the static spins.

In Fig. 7 we show velocity images of the previous experiment with four different methods of phase referencing. Figure 7a was calculated with a linear phase correction, in the read-out direction, of $\phi_c = P_a + 2P_b m/N$ applied to the five phase images used in linear regression. P_a and P_b for each phase image with flow were calculated from the static images taken with identical conditions. Similarly, Fig. 7b has a linear correction applied in both the read-out and the phase-encoding directions. In this case, the correction was $\phi_c = P_a + 2P_b m/N + 2P_{by} n/N$. For Fig. 7c, each phase image with no flow for a given value of m_1 was subtracted from the phase image with flow for the same value of m_1 and the velocity was calculated from these resultant images. In the previous methods, additional images with $V = 0$ cm/s were necessary for phase referencing. For Fig. 7d, we use the static spins present in one of the tubes in our

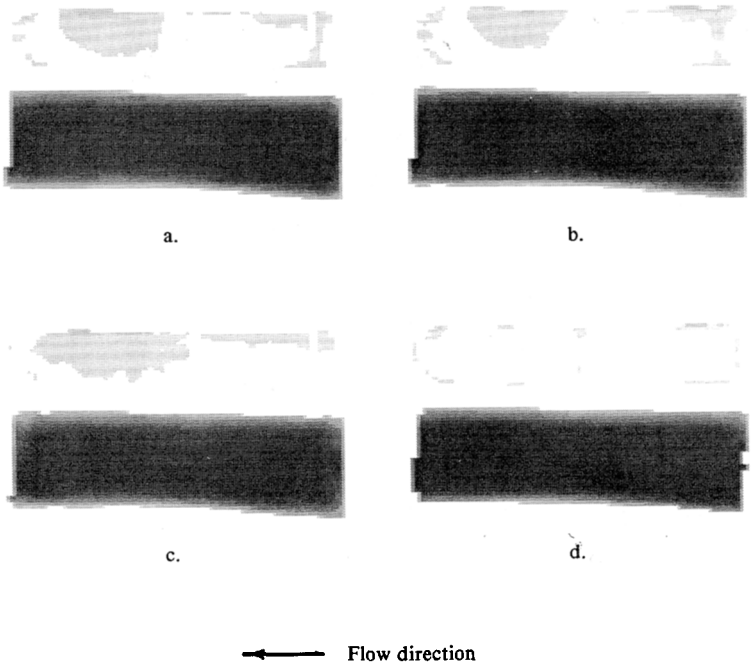

FIG. 7. Velocity images of the previous experiment with four different methods of phase referencing. Part a was calculated after a linear phase correction, in the read-out direction only, and was applied to the five phase images used in linear regression. Part b was obtained by a linear phase correction applied in both the read-out and the phase-encoding directions. In order to obtain c, the phase image with $V = 0$ cm/s was subtracted from phase images with flow for each value of m_1. In d, the linear phase correction was calculated from the phase image of the tube with static spins and the correction was then applied to the whole image.

model to calculate the constants P_a, P_b, and P_{by} needed for phase correction. The correction with these constants is then applied to the whole image.

In this comparison the method of using separate static spins as reference gave the best results (Fig. 7d). The other three methods gave similar results with the third method of subtracting phase images being slightly better, a conclusion which is not obvious from the scales chosen for plotting these figures. The last method was not only superior but has the added advantage of not requiring additional experiments. It does require the assumption that the phase correction calculated from the static spins can be extrapolated to the whole image.

Figure 8 shows velocity images and standard-deviation images of a bifurcation where the inlet tube and the two daughter tubes have an i.d. of 0.9 cm, a bifurcation angle of 60°, and an inlet average velocity of 16 cm/s (Re = 1440). In this experiment with the time-shifted velocity-encoding scheme shown in Fig. 3, G_3 was equal to 0.07 mT/cm, T_e was equal to 20 ms, and the velocity encoding was done by varying D_3 in steps of 100 μs, which gave a phase shift of 2° for a velocity of 1 cm/s. Five phase images were taken with different values of m_1 centered around $m_1 = 0$. Figures 8a, 8b, and 8c are the velocity images with Figs. 8d, 8e, and 8f being the corresponding

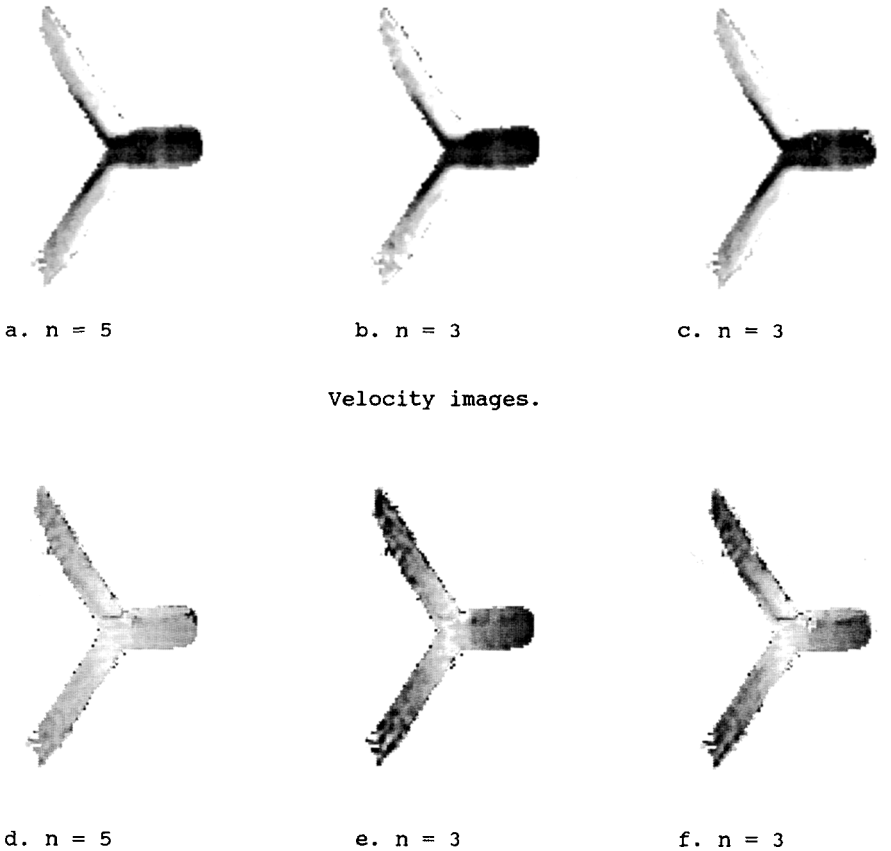

FIG. 8. The time-shifted pulse sequence of Fig. 3 was used to produce a projection velocity image of water flowing in a bifurcation with an average inlet flow velocity of 16 cm/s. In this figure we compare the effect of n, the number of images used in velocity calculations, on the velocity image and on hypothesis testing. Parts a, b, and c are the velocity images with d, e, and f being the corresponding standard-deviation images as calculated from different combinations of phase images. The intensity scale of the standard-deviation images has been increased four times as compared to the velocity image in order to bring out the details. Parts a and d were calculated from all the five phase images, b and e were calculated from the three smallest values of the phase-encoding steps, and c and f were calculated from the two extreme and the one central value ($m_1 = 0$) of velocity encoding. The horizontal scale is compressed compared to the vertical scale which makes the 60° bifurcation angle look like 90°.

standard-deviation images as calculated from different combinations of phase images. The intensity scale of the standard-deviation images has been increased four times as compared to the velocity image in order to bring out the details. Because the velocity encoding is along z, these velocity images have intensities proportional to the z com-

ponent of the velocity and not to the velocities along each segment of the bifurcation. A high-velocity flow was seen along the divider of the bifurcation whereas a thin region of negative flow was seen along the outer sides of the bifurcation as expected. The negative velocities have not been plotted here, although they are easily observed on the color monitor in our laboratory.

In Fig. 8 we observe the effect of n, the number of phase images used for calculating the velocity, on the velocity image and on the standard-deviation image. Figures 8a and 8d were calculated from all five phase images, Figs. 8b and 8e were calculated from the three middle values of the phase-encoding steps, and Figs. 8c and 8f were calculated from the two extreme and the one central value ($m_1 = 0$) of velocity encoding. The three velocity images are almost identical, with the velocity image of Fig. 8a ($n = 5$) being smoother and the $n = 3$ image with extreme values of m_1 (Fig. 8c) slightly better than that with small range of m_1 (Fig. 8b). The standard deviation was smallest for Fig. 8d ($n = 5$) with that of Fig. 8f ($n = 3$, with extreme values) slightly smaller than that of Fig. 8e ($n = 3$, with middle values). These observations are not surprising because the images with $n = 3$ are subsets of that of $n = 5$, and in the calculations with three images, the images with larger values of m_1 had the higher flow sensitivity. We have not addressed the problem of choosing the velocity-encoding step size (phase shift/cm/s) for the different phase images used in linear regression from the viewpoint of improving the accuracy of velocity images. A choice of a large value of m_1 is not always better, because depending on the velocity distribution in the voxel, phase cancellations can occur, leading to signal loss and less accurate phase calculations. If the range of expected velocities is known then it should be possible to select a set of m_1 values to optimize accuracy.

We have discussed two methods for reducing errors in velocity calculations caused by eddy-current-induced phase shifts. We first showed that these errors depend on the method of velocity encoding used. The example of changing the first moment of the gradient by shifting the π pulses had smaller errors than the corresponding sequence without π pulses, and we showed experimentally that it had smaller errors than the more usual amplitude-modulation pulse sequence. Next, we discussed the method of phase referencing which compensates for eddy-current-induced changes in the phase images which depend on m_1. This method is independent of the pulse sequence and can be used with all methods of velocity phase encoding. In fact, the eddy-current-induced phase-shift problems are corrected quite well by phase referencing and the particular method of velocity encoding chosen is not always that significant. However, the choice of a pulse sequence is important either if no phase calibration is done or if the experimental geometry causes phase referencing to perform poorly.

The random errors in phase were canceled by performing voxel-by-voxel linear regression of the data obtained by experimentally varying m_1. The linear regression produces an estimate of error in our velocity calculations and provides an objective criterion for deciding where the velocity should be considered zero, given the errors in the experiment. Unlike phase referencing, this method of linear regression does not correct for eddy-current-induced phase-shift errors, because they are also linear in m_1. It is a general method for obtaining velocity images and is applicable to all other methods of velocity phase encoding.

ACKNOWLEDGMENTS

We thank the reviewer for various useful suggestions and Dr. E. Fukushima for his patience and many discussions. A part of this work was supported by NIH Grant HL 31080 and a grant from the Flinn Foundation.

REFERENCES

1. V. J. WEDEEN, B. R. ROSEN, D. CHESLER, AND T. J. BRADY, *J. Comput. Assist. Tomogr.* **9,** 530 (1985).
2. C. L. DUMOULIN AND H. R. HART, JR., *Radiology* **161,** 717 (1986).
3. G. L. NAYLER, D. N. FIRMIN, AND D. B. LONGMORE, *J. Comput. Assist. Tomogr.* **10,** 715 (1986).
4. Z. H. CHO, C. H. OH, C. W. MUN, AND Y. S. KIM, *Magn. Reson. Med.* **3,** 857 (1986).
5. P. R. MORAN, *Magn. Reson. Imaging* **1,** 197 (1982).
6. P. MANSFIELD AND B. CHAPMAN, *J. Magn. Reson.* **72,** 211 (1987).
7. M. A. MORICH, D. A. LAMPMAN, W. R. DANNELS, AND F. T. D. GOLDIE, *IEEE Trans. Med. Imaging* **7,** 247 (1988); P. D. MAJORS, J. L. BLACKLEY, S. A. ALTOBELLI, A. CAPRIHAN, AND E. FUKUSHIMA, *J. Magn. Reson.* **87,** 548 (1990).
8. W. T. DIXON, *Radiology* **153,** 189 (1984).